

Mind the Prompt: A Novel Benchmark for Prompt-based Class-Agnostic Counting

Luca Ciampi¹, Nicola Messina¹, Matteo Pierucci², Giuseppe Amato¹, Marco Avvenuti², Fabrizio Falchi¹

¹CNR-ISTI, Pisa, Italy ²University of Pisa, Italy

luca.ciampi@isti.cnr.it, nicola.messina@isti.cnr.it

Abstract

Class-agnostic counting (CAC) is a recent task in computer vision that aims to estimate the number of instances of arbitrary object classes never seen during model training. With the recent advancement of robust vision-and-language foundation models, there is a growing interest in prompt-based CAC, where object categories to be counted can be specified using natural language. However, we identify significant limitations in current benchmarks for evaluating this task, which hinder both accurate assessment and the development of more effective solutions. Specifically, we argue that the current evaluation protocols do not measure the ability of the model to understand which object has to be counted. This is due to two main factors: (i) the shortcomings of CAC datasets, which primarily consist of images containing objects from a single class, and (ii) the limitations of current counting performance evaluators, which are based on traditional class-specific counting and focus solely on counting errors. To fill this gap, we introduce the Prompt-Aware Counting (PrACo) benchmark, which comprises two targeted tests, each accompanied by appropriate evaluation metrics. We evaluate state-of-the-art methods and demonstrate that, although some achieve impressive results on standard class-specific counting metrics, they exhibit a significant deficiency in understanding the input prompt, indicating the need for more careful training procedures or revised designs. The code for reproducing our results is available at <https://github.com/ciampluca/PrACo>.

1. Introduction

Object counting is the automated process of estimating the number of objects in still images or video frames [14]. Very recently, research about this task has undergone a detour towards class-agnostic counting (CAC) aiming at enumerating the instances of arbitrary object categories never seen during model training [21]. This new trend overcomes

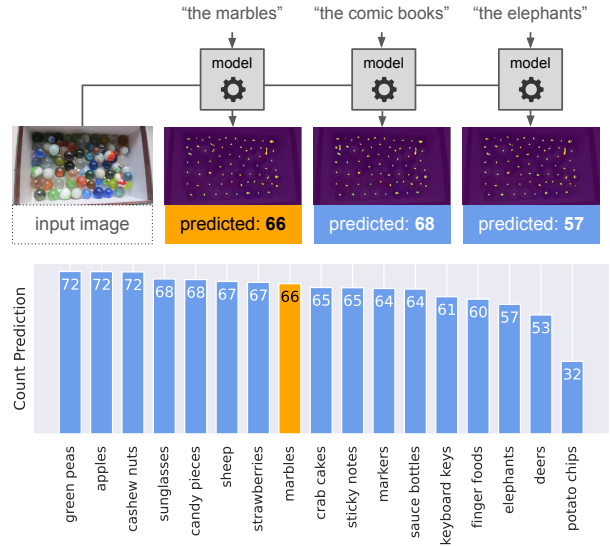


Figure 1. Prompt-guided counting models – CounTX [2] in this example – have problems in correctly understanding the user-provided text containing the class of objects to be counted. The confusion affects classes very well semantically separated – like *marbles* and *elephants*. The plot shows that classes exist that are not present in the image, for which state-of-the-art models estimate a higher count than the ground-truth class (in orange).

the limitations affecting class-specific counting methods that instead estimate the number of objects belonging to specific classes, requiring individually trained networks for each object type such as people [4, 10, 18, 22, 24], vehicles [1, 6, 29], or cells [5, 8]. In contrast, class-agnostic counting draws inspiration from humans’ instinctive ability to discern what merits counting when confronted with unfamiliar objects, and it enables users to specify arbitrary categories of interest at inference time without needing model retraining and gathering new annotated data.

Target object classes in CAC can be specified with visual exemplars, *i.e.*, bounding boxes surrounding object samples in the image [9, 17, 25, 27, 28], or with text prompts, *i.e.*,

textual object descriptions [2, 11, 12, 16, 19, 23, 26]. Even if current techniques exploiting visual exemplars outperform prompt-based methods, the latter setting is very appealing since it leverages the model’s natural language understanding, enhancing flexibility as less human intervention in the loop is required, *i.e.*, humans do not have to specify bounding box exemplars as input [2, 19].

However, in this paper, we figured out that current benchmarks for assessing prompt-based CAC approaches are affected by severe limitations hampering their proper evaluation and the development of new, more performing solutions. As shown in Fig. 1, we empirically verified that some state-of-the-art prompt-based CAC approaches are not always able to truly understand *which* object class has to be counted from the textual description, even if they reach top results on current performance evaluators. In contrast, they tend to count object instances belonging to the predominant class despite the prompt meaning. This is a critical failure in real-world scenarios if we imagine that such systems are usually deployed to count specific objects – *e.g.*, imagine a surveillance scenario in which the officer wants to count the number of pedestrians transiting on the street, but at that moment, only cars are present. We argue that this lack relies on two key factors: (i) the shortcomings affecting the main CAC datasets and (ii) the limitations affecting current counting performance evaluators. Specifically, most of the samples making up the datasets suitable for CAC contain objects belonging to a single class, making it hard to evaluate the model’s ability to discriminate different object classes within an image. Furthermore, the metrics exploited for measuring the performance of CAC models are inherited from class-specific counting and do not take into account some key factors of prompt-based CAC, focusing only on the counting error and disregarding to assess the model’s ability to understand the object category described by the textual prompt.

In this work, we propose Prompt-Aware Counting (PrACo), a novel benchmark designed to quantitatively evaluate the effectiveness of prompt-based CAC approaches in accurately interpreting input prompts. The benchmark includes two specific tests tackling the two above-mentioned limitations: (i) a *negative-label* test, which probes single-class images by using prompts that refer to absent classes, and (ii) a *mosaic* test, which evaluates artificially created images containing two distinct classes, with the prompt describing only one of them. Furthermore, PrACo comes with ad-hoc evaluation metrics specific for each of these two tests, overcoming the limitations affecting class-specific counting performance evaluators. To validate our new benchmark, we assess several recent SOTA prompt-based CAC techniques, and we show that some of them show a notable weakness in understanding the object class textual descriptions despite achieving top performance on stan-

dard class-specific metrics. This highlights the necessity for more refined training procedures or reconsideration of their architectural designs.

To summarize, we propose the following contributions:

- We propose PrACo, a novel benchmark aiming at assessing prompt-based CAC methods to overcome the limitations affecting current datasets and metrics hampering the development of more effective solutions.
- Contextually to this benchmark, we introduce a set of ad-hoc evaluation protocols and associated metrics to evaluate the models’ ability to count object classes described with natural language.
- We perform an experimental evaluation by exploiting PrACo showing that many recent state-of-the-art methods exhibit a remarkable deficiency in understanding the object to be counted although obtaining top results in standard class-specific counting metrics.

2. Related Work

2.1. Class-specific Object Counting

Class-specific object counting is one of the core tasks in computer vision due to its widespread applicability to many real-world applications. Thus, many methods have been proposed to count specific object categories, such as people [4, 10, 18, 22, 24], cars [1, 6, 29], insects [3, 7], or cells [5, 8]. Approaches that regress and sum density maps have emerged to be more accurate in crowded scenarios [3, 4, 10, 18, 22, 24] than techniques relying on prior detection of object instances [1, 6]. Either way, the main drawback of class-specific counting lies in requiring individually trained networks and, consequently, labeled datasets for each object type.

2.2. Prompt-based Class-agnostic Counting

Very recently, class-agnostic counting (CAC) has generalized class-specific counting to open-world settings, where users can specify arbitrary object classes never seen during model training [21]. Specifically, the object category to be counted is selected at inference time by exploiting (i) visual exemplars, *i.e.*, some bounding boxes around the objects of interest within the same input image [9, 17, 25, 27, 28], or (ii) textual prompts, *i.e.*, natural-language descriptions of the object class [2, 11, 12, 16, 19, 23, 26]. The first setting provides the best performance: methods such as CACViT [25], SSD [27], CounTR [17], LOCA [9], and SAFECOUNT [28] reach state-of-the-art in all CAC benchmarks. In contrast, prompt-based CAC approaches allow the input of object properties through text, and they are particularly appealing since they enhance overall flexibility.

Most of the state-of-the-art prompt-based CAC approaches rely on vision-language foundation models that

map text-image pairs to a joint embedding space; the produced features are then passed to a decoder in charge of producing density maps. The authors in [26] trained a conditional variational autoencoder (VAE) based on the popular CLIP model [20] to generate visual exemplar prototypes conditioned with their semantic embedding encoded in the provided category name; prototypes are then used with existing visual exemplar-based CAC techniques. Concurrently, [2] proposed CounTX that instead is trained end-to-end and produces object counts directly, skipping the intermediate visual exemplar proposal step; furthermore, it accepts a more detailed specification of the target object to count (rather than simply using a class name). More in detail, it is built on top of a CLIP model, where a feature interaction module is used to mine the similarities between image patches and class descriptions. Similarly, CLIP-Count [11] relies on CLIP to align the text embedding with dense visual features. However, in this paper, the authors also designed a hierarchical patch-text interaction module to propagate semantic information across different resolution levels of visual features. Another similar CLIP-based model trained end-to-end is represented by VL-Counter [12]. Here, the authors incorporated three modules to efficiently finetune CLIP for the counting task and to exploit intermediate features across different encoding layers of CLIP in the decoding stage. Very recently, DAVE [19] proposed a two-stage detect-and-verify paradigm. In the first stage, they estimate a high-recall set of candidate detections, which are then analyzed and filtered in the second verification step, relying on unsupervised clustering and CLIP embedding. Differently from the above-described architectures, TFPOC [23] employed a detection-based technique, leveraging the popular SAM [13] for instance segmentation. The authors proposed a two-stage approach. In the first stage, they exploited CLIP-Surgery [15], an enhanced version of CLIP, to produce visual exemplar prototypes by computing the similarity between images and text representations. In the second step, they computed a similarity map by using cosine similarity between image features and the masks corresponding to the reference objects produced by SAM prompted with the bounding boxes from the first stage. However, in this work, we empirically demonstrate that these prompt-based CAC models are not always able to truly understand the object category to be counted from the textual description, tending simply to the most predominant object class instead.

2.3. Dataset and Metrics

The gold standard dataset for CAC is FSC-147 [21]. It comprises 6,135 images covering 147 object categories. Annotations consist of dots over the approximate centroids of each object instance, as usual for the counting task – ground truth density maps are created by superimposing

Gaussian kernels centered on these dots. Furthermore, the authors provided three bounding boxes per image that localize the exemplars and the natural language name of the object category to which they belong – the category is unique for each image, and it has been chosen arbitrarily if multiple categories were present. However, cases in which multiple object categories are present in the same image are just a few, and this represents an inherent limitation of FSC-147, making it hard to evaluate the model’s ability to discriminate different object classes within an image.

Standard counting metrics in the literature are the Mean Absolute Error (MAE) and the Root Mean Squared Error (RMSE), defined as $MAE = \frac{1}{N} \sum_{n=1}^N |\tilde{c}_n - c_n|$ and $RMSE = \sqrt{\frac{1}{N} \sum_{n=1}^N (\tilde{c}_n - c_n)^2}$, where N is the number of test images, and \tilde{c}_n and c_n are the ground truth and predicted counts, respectively. However, these evaluators were inherited from the class-specific counting task and exhibit severe limitations particularly evident in prompt-based CAC. Specifically, they do not take into account *which* object category has to be counted nor the model’s ability to understand the provided textual prompt.

3. The PrACo Benchmark

3.1. Overview

Standard class-specific counting benchmarks have several limitations when used to evaluate prompt-based CAC models. In this context, it is essential to not only measure the model’s accuracy in estimating the number of object instances but also to verify whether the model correctly identifies *which* object should be counted based on the given textual prompt.

We assume to have a collection of N tuples $\mathcal{X} = \{(I_1, P_1), (I_2, P_2), \dots, (I_N, P_N)\}$, where I_i is an image and P_i is the class name of the objects within I_i , *i.e.* each image contains objects belonging to only a single class. We define P_i as the *positive* class and all the $\{P_j\}_{j \neq i}$ as the *negative* classes for the given I_i . Without loss of generality and for simplifying the formalisms, we are assuming that each class appears in only one image of the dataset, although in real-world scenarios, datasets collect multiple images for the same class of objects.

On this common structure, PrACo introduces two test suites, which are detailed in the following sections: (i) a *negative-label* test and (ii) a *mosaic* test.

3.2. Negative-label test

The *negative-label* test evaluates single-class images by prompting the model with textual descriptions referring to absent object classes. Formally, we are given a counting model $\mathcal{M}(I, P)$, which takes as input the image I and an arbitrary prompt P containing the class to be counted and

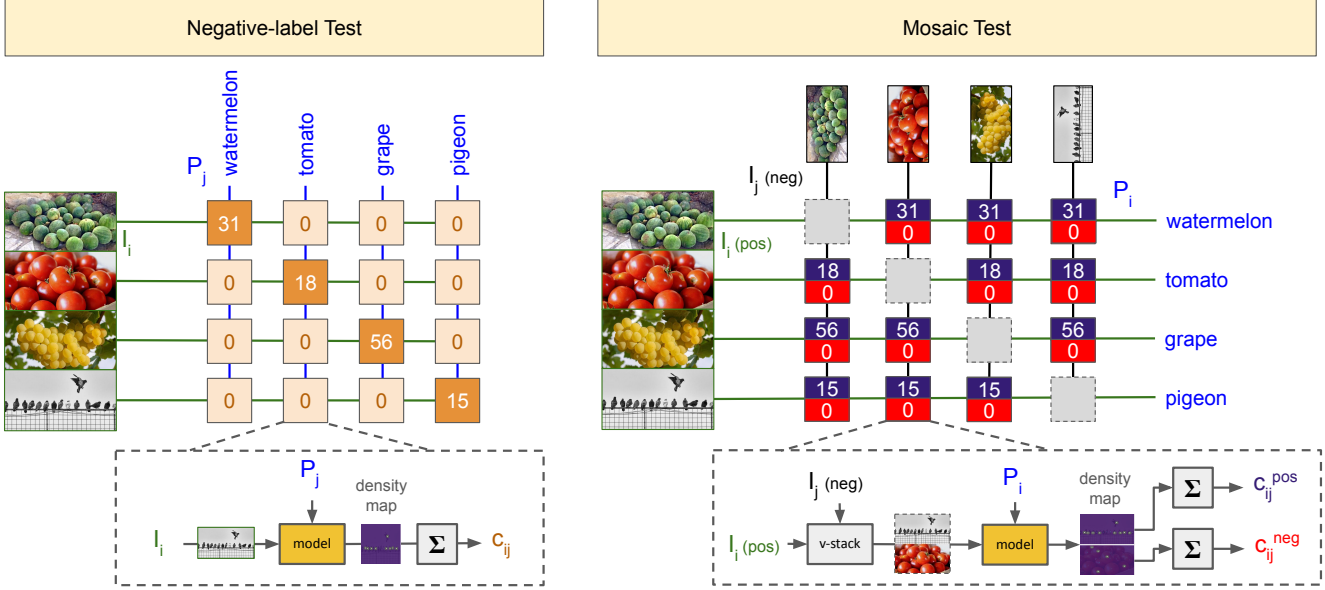


Figure 2. Inference schemas for the *negative-label test* (on the left) and the *mosaic test* (on the right). The numbers reported in the boxes show the ideal model outcomes: for the negative-label test, the diagonal of the shown matrix should be filled with the ground-truth object counts and with zeros elsewhere; for the mosaic test, each mosaic outcome should contain the ground-truth counts on the top – which is the same for each row of the shown matrix – and zeros on the bottoms. In the dotted boxes on the bottom, we report a schema of the inference procedures needed for computing each entry of the two matrices.

outputs an estimated count for that class. For all the elements $\{I_i, P_j\}_{i,j=1}^N$, we compute $c_{ij} = \mathcal{M}(I_i, P_j)$ to obtain the count that the model predicts for each image when prompted with all the available classes in the dataset. In order for this test to perfectly succeed, we would ideally require to achieve the following c_{ij} configuration:

$$c_{ij} = \begin{cases} \tilde{c}_i, & \text{if } i = j \\ 0, & \text{if } i \neq j \end{cases}, \quad (1)$$

where \tilde{c}_i is the ground truth count for the image I_i . In other words, other than solely checking that the model correctly estimates the number of objects for the positive class – which is what classical counting metrics check – we are also required to verify that the model estimates a near-zero count when prompted with negative classes. The ideal situation is illustrated in the left part of Figure 2. To quantitatively assess this test, we introduce two metrics that, unlike the classical counting metrics, try to quantify the error caused by counting the wrong objects.

Normalized Mean of Negative predictions (NMN). NMN is the absolute counting error computed by prompting the model with the negative classes, normalized by the ground truth of the positive class. It is computed as follows

(more details in the supplementary):

$$\text{NMN} = \frac{1}{N(N-1)} \sum_{i=1}^N \frac{1}{\tilde{c}_i} \sum_{\substack{j=1 \\ j \neq i}}^N c_{ij} \quad (2)$$

Notice that the reason for normalizing the average of the negative counts by the ground truth of the positive class is given by the assumption that having more items in the image also causes the model to increase the estimate of non-present classes. Therefore, the normalization factor $1/\tilde{c}_i$ plays the role of relativizing the error – in other words, we suppose that counting 10 *dogs* in an image showing 1000 *people* is a negligible error. The lower the NMN value, the better the resulting model.

Positive Class Count Nearness (PCCN). PCCN is an aggregate measure defined as the percentage of samples in the dataset where the model produces a positive count estimate that is nearer to the ground truth with respect to the mean of the negative classes. Formally, it is defined as follows:

$$\text{PCCN} = \frac{1}{N} \sum_{i=1}^N \mathbb{I}(d_i^{\text{pos}} < d_i^{\text{neg}}) \cdot 100\% \quad (3)$$

where $d_i^{\text{neg}} = |\frac{1}{N} \sum_{\substack{j=1 \\ j \neq i}}^N c_{ij} - \tilde{c}_i|$ is the absolute difference between the mean of the model’s predictions based on the

negative labels and the ground truth count for the i -th image, $d_i^{\text{pos}} = |c_{ii} - \tilde{c}_i|$ is the absolute difference between the model’s prediction based on the positive label and the ground truth count for the i -th image, and $\mathbb{I}(\cdot)$ is the indicator function, which equals 1 if the condition inside it is true, and 0 otherwise. Unlike NMN, this metric gives an interesting global view by mixing positive and negative label predictions. It provides an overall quantitative assessment of strong failures in the model. In fact, a mean negative estimate closer to ground truth than the positive one may signify that the model is strongly biased to count most of the negative classes instead of the positive one, which in turn may be due to the model completely losing the semantics of the given prompt. The higher the WPR, the better the resulting model.

3.3. Mosaic test

Differently from the *negative* test, in the *mosaic* test, counting models are asked to count objects in a query image where two classes are present. The objective is, therefore, to quantitatively assess the ability of the model to distinguish between the correct class and another randomly chosen class that is present in the same image. This test wants to emulate real case scenarios in which an image contains multiple object classes, and the model is requested to count only one. Unfortunately, suitable real-world counting datasets annotated with multiple classes are difficult to obtain. Therefore, from largely used datasets like FSC-147 containing images with a single class of objects, we artificially create multi-class images by concatenating a positive class image with a negative class one, similarly to [2].

Specifically, we are given all the possible pairs of images from the dataset $\{I_i, I_j\}_{i,j=1}^N$, and the positive class P_i of the image I_i . We call I_i and I_j the *positive* and the *negative* images, respectively. We create the mosaics $I_{ij}^{\text{coll}} = \text{vstack}(I_i, I_j)$, which are obtained by stacking the positive image on top of the negative ones on the y axis. We then perform inference with the target counting model using the positive label P_i – associated with the top image in the collage – in the following way: $c_{ij}^{\text{pos}}, c_{ij}^{\text{neg}} = \mathcal{M}(I_{ij}^{\text{coll}}, P_i)$. Specifically, the returned c_{ij}^{pos} is the count relative to the top part of the collage, while c_{ij}^{neg} is the count relative to the below image of the collage. This can be easily obtained from most density-based models, as it is sufficient to cut the output density map in half along the y -axis and integrate them separately to obtain the respective positive and negative counts. Notice that, in this test, the positive count c_{ij}^{pos} depends on j as well (the different negatives), as the model may be distracted to count the positive instances depending on which negative image is present in the bottom part of the mosaic. Similarly to the negative test, we would require c_{ij}^{pos} to converge to the ground truth count, while c_{ij}^{neg} to converge

identically to zero, as the model (i) should not be fooled by the negative examples while attending the positive instances and (ii) should not count any of the negative instances in the collage. We summarize this inference procedure in the right part of Figure 2.

The metrics for assessing such behavior should evidence whether the model correctly counts only the correct class while ignoring elements from the negative one. Due to the presence of positive and negative instances for each probed mosaic, this task has many similarities with *object detection*, where we may have correct and incorrect detections. In this scenario, usually, the performance is computed by using *precision* – which accounts for the number of correct predictions among all the model outputs – and *recall* – which represents the fraction of correct instances that were retrieved among all the ground-truth correct instances. Differently from the detection case, in our scenario, we do not have precise information about the correctness of each proposed instance, given that we do not know – and we are not requested to know – the precise localization of each instance within the image, as we are only interested in the final aggregated count for the provided class of objects. Such information could be partially recovered from the two output counts c_{ij}^{pos} and c_{ij}^{neg} by making some reasonable assumptions that we will present in the following paragraphs, where we present the precision-recall adapted metrics for the counting task.

Counting Precision and Recall. Classical precision and recall metrics used in detection scenarios are defined through true positive count (TP), false positive count (FP), and false negative count (FN). In the counting scenario, we do not have an indication of whether a single instance is correct or not, as we only have the estimated global count for the provided class of objects. We only know that correct objects are only present in the positive image I_i and that the negative image I_j only contains incorrect examples for the prompt P_i . To adapt precision and recall metrics to the counting case, we make a simple assumption. Specifically, for the counting contributions c_{ij}^{pos} from the positive image I_i , we never have FN instances. We may only have FPs in the case where the predicted count $c_{ij}^{\text{pos}} > \tilde{c}_i$, where \tilde{c}_i is the ground truth count for the positive instances in I_i . In such a case, we are assuming that the instances exceeding the correct count are false predictions. Also note that all the contributions c_{ij}^{neg} coming from the negative image I_j are surely FPs, as in such cases, the model is erroneously counting the incorrect instances in the lower part of the mosaic. Figure 3 shows an example of the computation of TPs and FPs for adapting the precision and recall detection metrics to the counting scenario.

Under the above considerations and assumptions, we obtain that *counting precision* (CntP) and *counting recall*

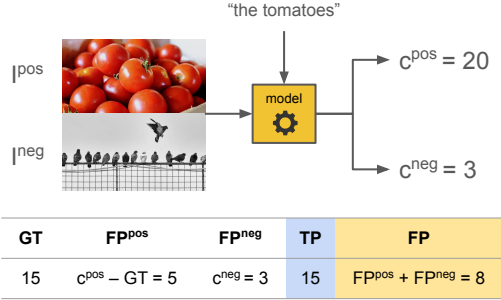


Figure 3. Example of the derivation of TPs and FPs in the mosaic scenario. In the shown case where the model predicts $c^{\text{pos}} = 3$ and $c^{\text{neg}} = 20$, the number of estimated true positives is bounded to the ground-truth value (15). The remaining 5 counted elements are considered false positives from the positive image ($\text{FP}^{\text{pos}} = 5$), which are then merged with the false positives from the negative image ($\text{FP}^{\text{neg}} = c^{\text{neg}} = 3$), to obtain a total of 8 FPs.

(CntR), for each mosaic image, can be defined as follows:

$$\text{CntP} = \frac{1}{N(N-1)} \sum_{\substack{i,j=1 \\ j \neq i}}^N \frac{\min(c_{ij}^{\text{pos}}, \tilde{c}_i)}{c_{ij}^{\text{pos}} + c_{ij}^{\text{neg}}} \quad (4)$$

$$\text{CntR} = \frac{1}{N(N-1)} \sum_{\substack{i,j=1 \\ j \neq i}}^N \frac{\min(c_{ij}^{\text{pos}}, \tilde{c}_i)}{\tilde{c}_i} \quad (5)$$

We refer the reader to the supplementary material for the derivation of such expressions from the idea shown in Figure 3.

The *counting recall* metric is useful to understand if the model can correctly estimate the number of objects belonging to the positive class. Interestingly, in the range $c_{ij}^{\text{pos}} < \tilde{c}_i$, it correlates negatively with the MAPE error metric – clamping to 1 when the predicted count is greater than the ground truth. Therefore, CntR carries information partially correlated with class-specific counting metrics, except that the model is also exposed to negative examples that may alter the number of predicted instances.

Differently, the *counting precision* metric is useful to understand if the model is erroneously including in the count estimation also objects belonging to classes not specified by the textual prompt and present in the negative image I_j . Specifically, it is sensitive to the FPs found both in the positive image I_i – the counting excess with respect to the ground-truth – and in the negative image I_j – where every instance is considered a FP.

Counting Balanced F-score. A common way to aggregate precision and recall to obtain a single indicator is the F-score, which is defined as the harmonic mean of the two metrics. We therefore derive a *counting F1-score* (CntF1) indicator, as follows:

$$\text{CntF1} = 2 \cdot \frac{\text{CntP} \cdot \text{CntR}}{\text{CntP} + \text{CntR}} \quad (6)$$

This metric is useful for comparing the overall performance of the CAC models, taking into consideration objects belonging both to desired and undesired classes.

4. Experimental Evaluation

4.1. Dataset and Methods

Dataset. Our benchmark is based on the widely-used FSC-147 dataset, designed for class-agnostic object counting that includes a total of 6,135 images. The training portion of FSC-147 consists of images from 89 distinct categories, while both the validation and test sets are composed of images from 29 different categories. Since, in our work, we probe pre-trained state-of-the-art models, we only consider the test and validation splits composed of 1190 and 1286 images, respectively. Notably, there is no overlap between the classes in the training, validation, and test sets, positioning FSC-147 as an open-world dataset. Although most of the images in FSC-147 contain only one class of objects, there are a few containing multiple classes. In order to avoid interfering with our negative-examples evaluation, we filter all the images from test and validation sets where there are more than two object classes. In this way, we are sure that there are no false positive contributions from the other classes in the same image.

Probed Methods. We place under the spotlight six different state-of-the-art prompt-based CAC methods: CounTX [2], CLIP-Count [11], TFPOC [23], VLCounter [12], and DAVE [19]. Specifically, CounTX, CLIP-Count, and VLCounter directly estimate density-maps end-to-end by fine-tuning CLIP and conditioning the density-map generation on the CLIP embedding of the desired object class. Instead, TFPOC and DAVE employ two-stage approaches that detect all the objects in the image and then filter them based on the input textual prompt.

Implementation Details. We employed the code and the pre-trained models provided by the authors. We stuck to the original image preprocessing pipelines, and we kept the author’s chosen hyperparameters and prompting schema. We only needed to adjust the DAVE inference procedure to behave correctly on our benchmark. In the supplementary material, we better comment on this small yet important modification, also reporting the PrACo performance of the original DAVE implementation.

4.2. Results

Quantitative Results on Negative and Mosaic Tests. We report the results for both the test and validation splits

Table 1. Results on the **test set** of FSC147 on both PrACo metrics (negative and mosaics tests) and on classic metrics.

Method	Negative Test		Mosaic Test			Classic	
	NMN ↓	PCCN ↑	CntP ↑	CntR ↑	CntF1 ↑	MAE ↓	RMSE ↓
CounTX [2] (BMVC '23)	0.95	64.51	0.686	0.712	0.630	15.92	106.89
CLIP-Count [11] (ACM MM '23)	1.27	38.13	0.495	0.761	0.554	17.59	109.97
VLCounter [12] (AAAI '24)	1.15	53.36	0.517	0.781	0.577	17.02	106.93
TFPOC [23] (WACV '24)	0.75	66.04	0.687	0.848	0.696	24.79	138.11
DAVE [19] (CVPR '24)	0.08	97.62	0.843	0.799	0.790	15.23	103.53

Table 2. Results on the **validation set** of FSC147 on both PrACo metrics (negative and mosaics tests) and on classic metrics.

Method	Negative Test		Mosaic Test			Classic	
	NMN ↓	PCCN ↑	CntP ↑	CntR ↑	CntF1 ↑	MAE ↓	RMSE ↓
CounTX [2] (BMVC '23)	0.87	69.79	0.664	0.658	0.579	17.27	66.37
CLIP-Count [11] (ACM MM '23)	1.24	48.11	0.488	0.702	0.522	18.90	66.75
VLCounter [12] (AAAI '24)	1.07	62.70	0.520	0.741	0.561	18.09	65.59
TFPOC [23] (WACV '24)	0.67	62.62	0.723	0.757	0.656	32.84	110.60
DAVE [19] (CVPR '24)	0.13	95.90	0.819	0.751	0.757	16.58	54.73

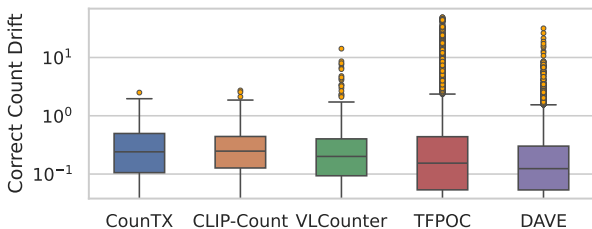


Figure 4. Boxplot showing the distribution of the correct count drifts of the different models. Despite the lower mean value, TFPOC and DAVE show a consistent number of outliers, revealing that they may catastrophically fail in some specific conditions.

in Tables 1 and 2, respectively. As we can notice, although the methods achieve remarkable performance on standard counting error measures (MAE and RMSE), the outcome is quite heterogeneous on the PrACo metrics. Notably, the negative test on one-stage methods like CounTX, CLIP-Count, and VLCounter shows that the average negative count is comparable to the ground-truth count of the correct class ($NMN \approx 1$), with CLIP-Count and VLCount achieving $NMN > 1$. This trend is further confirmed by the PCCN metric, where CLIP-Count has the correct estimate nearer to the ground-truth only 38% of the times on the test set. Instead, the two-stage detectors TFPOC and DAVE achieve the best performance on the negative test. The same trends are mostly confirmed on the mosaic test. Specifically, while the CntR metric only increments by around

12% between the worst-performing method (CounTX) and the best-performing one (DAVE), the CntP shows a notable increase, from 0.517 of VLCounter to 0.843 of DAVE, which is an improvement of around 63%. This shows how the methods, despite being mostly able to count the correct class, have a highly heterogeneous behavior with respect to the negative images within the mosaics. It also worth noticing that more recent methods do not always improve on the PrACo metrics, meaning that this aspect is still largely underestimated. At the same time, it is interesting to observe how TFPOC, a training-free model obtaining less competitive results on classic counting metrics, can instead defeat older learning-based CAC models on the proposed metrics.

Correct Count Drift. From the mosaic test, it is also interesting to understand how the various models drift the estimate about the positive class c_{ij}^{pos} when changing the negative image I_j . In other words, we would like to estimate the *confusion* of the model when it is requested to count a given class, but objects of another class are present in the image. In Figure 4, we report, for each model, the distribution of the quantity $\left\{ \frac{|c_{ij}^{pos} - c_{ii}|}{c_{ii}} \right\}_{i,j=1}^N$, which encodes the normalized absolute error between the estimate of the model when only presented with the correct class as estimated in the negative test (c_{ii}) and the estimate of the model when presented with all the mosaics constructed with positive image I_i on the top (c_{ij}^{pos}). As we can notice, although DAVE achieves the lowest drift, it also presents many possibly problematic outliers. This may be due to the verification module, which

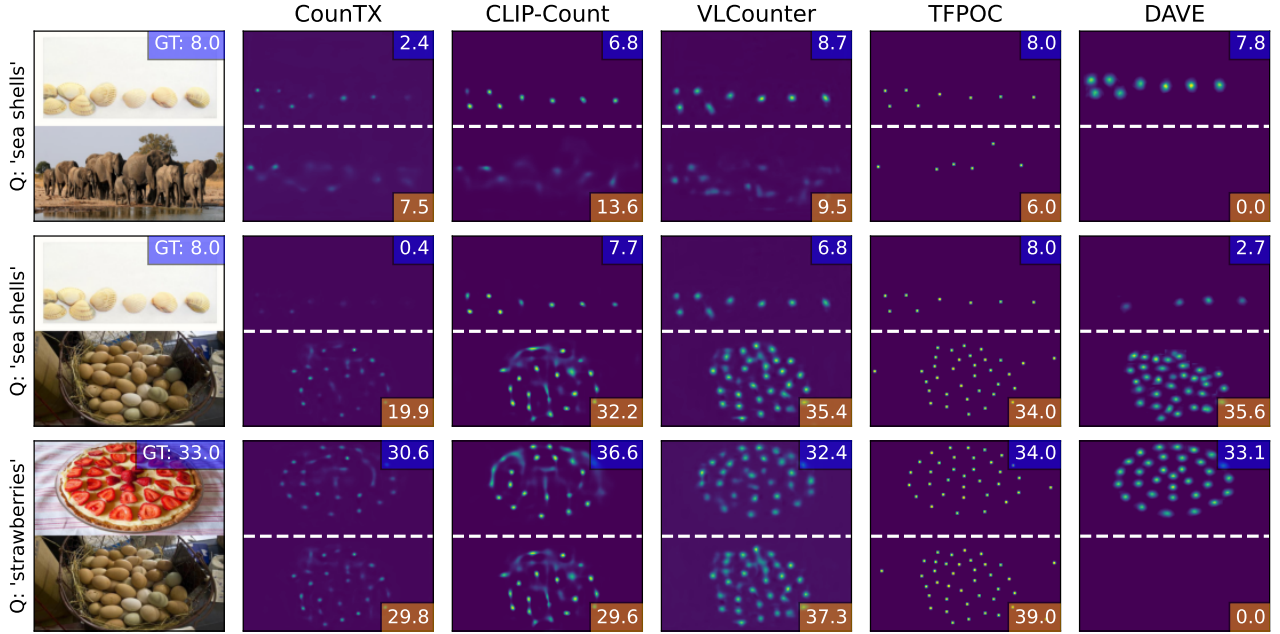


Figure 5. This figure shows, for each model, the output density maps for three different (*mosaic, input prompt*) pairs. In each figure, the count reported in the blue box is c_{ij}^{pos} , while the count reported in the red box corresponds to c_{ij}^{neg} . We can notice how the models incorrectly attend to the instances from the negative image in the mosaic, although most of them provide a good estimate for the positive instances in the upper image of the mosaic.

incorrectly assigns the positive label to the cluster obtained from the objects from the negative image. Despite having a higher mean drift, the other methods – especially CounTX and CLIP-Count – show fewer outliers. This signifies that, although these methods wrongly count the negative classes, the count relative to the positive part of the mosaic is less dependent on the number of negative instances from the bottom image of the mosaic. This insight further raises the attention to effective two-stage methods that, despite being very effective in discriminating the different classes, may catastrophically fail in some specific scenarios.

Qualitative Results. In Figure 5, we show some qualitative results from the various methods examined through the lenses of the mosaic test. The lack of a proper understanding of the correct class to count is largely deducible from the reported density maps. While many methods correctly estimate the positive class on the top of the mosaics, most of the models give a non-zero count prediction of the negative instances from the negative images. We can notice how DAVE, in the first and last rows, correctly ignores the negative instances, exactly estimating zero objects. However, its second-stage verification approach may occasionally fail in a catastrophic manner, assigning the label to all the instances of the negative class, as shown in the second reported example. Although the mosaic test already gives

many insights into the failure modes of the probed SOTA models, in the supplementary material, we also report some qualitative results from the negative test.

5. Conclusions

In this paper, we introduced Prompt-Aware Counting (PrACo), a novel benchmark composed of two targeted test suites specifically designed to address the limitations of current evaluation systems for prompt-based class-agnostic counting (CAC).

Our evaluation of several recent state-of-the-art CAC methods revealed significant performance gaps, particularly in the models’ ability to handle negative and multi-class scenarios. While two-stage models like DAVE generally outperformed one-stage models on the negative test, they still exhibited notable weaknesses, particularly in the mosaic test, where they sometimes struggled with false positives from the negative images.

These findings suggest that SOTA models, despite their success on standard metrics, require more careful designs and better training procedures to improve their understanding of textual prompts. We hope PrACo provides a foundation for a more comprehensive evaluation and opens the door for developing more robust methods in the near future.

References

- [1] Giuseppe Amato, Luca Ciampi, Fabrizio Falchi, and Claudio Gennaro. Counting vehicles with deep learning in onboard uav imagery. In *2019 IEEE Symposium on Computers and Communications (ISCC)*, pages 1–6, 2019. 1, 2
- [2] N. Amini-Naieni, K. Amini-Naieni, T. Han, and A. Zisserman. Open-world text-specified object counting. In *BMVC*, 2023. 1, 2, 3, 5, 6, 7
- [3] Arantza Bereciartua-Pérez, Laura Gómez, Artzai Picón, Ramón Navarra-Mestre, Christian Klukas, and Till Eggers. Insect counting through deep learning-based density maps estimation. *Computers and Electronics in Agriculture*, 197:106933, 2022. 2
- [4] Xinkun Cao, Zhipeng Wang, Yanyun Zhao, and Fei Su. Scale aggregation network for accurate and efficient crowd counting. In Vittorio Ferrari, Martial Hebert, Cristian Sminchisescu, and Yair Weiss, editors, *ECCV*, pages 757–773, Cham, 2018. Springer International Publishing. 1, 2
- [5] Luca Ciampi, Fabio Carrara, Valentino Totaro, Raffaele Mazziotti, Leonardo Lupori, Carlos Santiago, Giuseppe Amato, Tommaso Pizzorusso, and Claudio Gennaro. Learning to count biological structures with raters’ uncertainty. *Medical Image Analysis*, 80:102500, 2022. 1, 2
- [6] Luca Ciampi, Claudio Gennaro, Fabio Carrara, Fabrizio Falchi, Claudio Vairo, and Giuseppe Amato. Multi-camera vehicle counting using edge-ai. *Expert Systems with Applications*, 207:117929, 2022. 1, 2
- [7] Luca Ciampi, Valeria Zeni, Luca Incrocci, Angelo Canale, Giovanni Benelli, Fabrizio Falchi, Giuseppe Amato, and Stefano Chessa. A deep learning-based pipeline for whitefly pest abundance estimation on chromotropic sticky traps. *Ecological Informatics*, 78:102384, 2023. 2
- [8] Joseph Paul Cohen, Geneviève Boucher, Craig A. Glastonbury, Henry Z. Lo, and Yoshua Bengio. Count-ception: Counting by fully convolutional redundant counting. In *2017 IEEE International Conference on Computer Vision Workshops (ICCVW)*, pages 18–26, 2017. 1, 2
- [9] Nikola Dukic, Alan Lukežic, Vitjan Zavrtnik, and Matej Kristan. A low-shot object counting network with iterative prototype adaptation. In *ICCV, Paris, France, October 1-6, 2023*, pages 18826–18835. IEEE, 2023. 1, 2
- [10] Mohammad Hossain, Mehrdad Hosseinzadeh, Omit Chanda, and Yang Wang. Crowd counting using scale-aware attention networks. In *2019 IEEE Winter Conference on Applications of Computer Vision (WACV)*, pages 1280–1288, 2019. 1, 2
- [11] Ruixiang Jiang, Lingbo Liu, and Changwen Chen. Clip-count: Towards text-guided zero-shot object counting. In *ACM MM*, MM ’23, page 4535–4545, New York, NY, USA, 2023. Association for Computing Machinery. 2, 3, 6, 7
- [12] Seunggu Kang, WonJun Moon, Euiyeon Kim, and Jae-Pil Heo. Vlcounter: Text-aware visual representation for zero-shot object counting. *AAAI*, 38(3):2714–2722, Mar. 2024. 2, 3, 6, 7
- [13] Alexander Kirillov, Eric Mintun, Nikhila Ravi, Hanzi Mao, Chloe Rolland, Laura Gustafson, Tete Xiao, Spencer Whitehead, Alexander C. Berg, Wan-Yen Lo, Piotr Dollár, and Ross Girshick. Segment anything, 2023. 3, 13
- [14] Victor Lempitsky and Andrew Zisserman. Learning to count objects in images. In J. Lafferty, C. Williams, J. Shawe-Taylor, R. Zemel, and A. Culotta, editors, *NeurIPS*, volume 23. Curran Associates, Inc., 2010. 1
- [15] Yi Li, Hualiang Wang, Yiqun Duan, and Xiaomeng Li. CLIP surgery for better explainability with enhancement in open-vocabulary tasks. *CoRR*, abs/2304.05653, 2023. 3
- [16] Wei Lin and Antoni B. Chan. A fixed-point approach to unified prompt-based counting. *AAAI*, 38(4):3468–3476, Mar. 2024. 2
- [17] Chang Liu, Yujie Zhong, Andrew Zisserman, and Weidi Xie. Countr: Transformer-based generalised visual counting. In *BMVC*. BMVA Press, 2022. 1, 2
- [18] Weizhe Liu, Mathieu Salzmann, and Pascal Fua. Context-aware crowd counting. In *CVPR*, pages 5094–5103, 2019. 1, 2
- [19] Jer Pelhan, Alan Lukežič, Vitjan Zavrtnik, and Matej Kristan. Dave - a detect-and-verify paradigm for low-shot counting. In *CVPR*, pages 23293–23302, June 2024. 2, 3, 6, 7
- [20] Alec Radford, Jong Wook Kim, Chris Hallacy, Aditya Ramesh, Gabriel Goh, Sandhini Agarwal, Girish Sastry, Amanda Askell, Pamela Mishkin, Jack Clark, Gretchen Krueger, and Ilya Sutskever. Learning transferable visual models from natural language supervision. In *Proceedings of the 38th International Conference on Machine Learning, ICML 2021, 18-24 July 2021, Virtual Event*, volume 139, pages 8748–8763. PMLR, 2021. 3
- [21] V. Ranjan, U. Sharma, T. Nguyen, and M. Hoai. Learning to count everything. In *CVPR*, pages 3393–3402, Los Alamitos, CA, USA, jun 2021. IEEE Computer Society. 1, 2, 3
- [22] Deepak Babu Sam, Shiv Surya, and R. Venkatesh Babu. Switching convolutional neural network for crowd counting. In *CVPR*, pages 4031–4039, 2017. 1, 2
- [23] Z. Shi, Y. Sun, and M. Zhang. Training-free object counting with prompts. In *2024 IEEE/CVF Winter Conference on Applications of Computer Vision (WACV)*, pages 322–330, Los Alamitos, CA, USA, jan 2024. IEEE Computer Society. 2, 3, 6, 7
- [24] Zenglin Shi, Le Zhang, Yun Liu, Xiaofeng Cao, Yangdong Ye, Ming-Ming Cheng, and Guoyan Zheng. Crowd counting with deep negative correlation learning. In *CVPR*, pages 5382–5390, 2018. 1, 2
- [25] Zhicheng Wang, Liwen Xiao, Zhiguo Cao, and Hao Lu. Vision transformer off-the-shelf: A surprising baseline for few-shot class-agnostic counting. *AAAI*, 38(6):5832–5840, Mar. 2024. 1, 2
- [26] Jingyi Xu, Hieu Le, Vu Nguyen, Viresh Ranjan, and Dimitris Samaras. Zero-shot object counting. In *CVPR*, pages 15548–15557, 2023. 2, 3
- [27] Yuanwu Xu, Feifan Song, and Haofeng Zhang. Learning spatial similarity distribution for few-shot object counting. *CoRR*, abs/2405.11770, 2024. 1, 2
- [28] Zhiyuan You, Kai Yang, Wenhan Luo, Xin Lu, Lei Cui, and Xinyi Le. Few-shot object counting with similarity-aware feature enhancement. In *2023 IEEE Winter Conference on Applications of Computer Vision (WACV)*, pages 6304–6313, 2023. 1, 2

- [29] Shanghang Zhang, Guanhang Wu, João P. Costeira, and José M. F. Moura. Fcn-rlstm: Deep spatio-temporal neural networks for vehicle counting in city cameras. In *ICCV*, pages 3687–3696, 2017. [1](#), [2](#)

Mind the Prompt: A Novel Benchmark for Prompt-based Class-Agnostic Counting

Supplementary Material

A. Derivation of Counting Precision and Recall

In this section, we better detail the derivation of Eqs. 4 and 5 within the paper, *i.e.*, the formulas for computing *counting precision* and *counting recall* starting from the inferred quantities c^{pos} and c^{neg} concerning the mosaic test. For ease of notation, here we omit the indexes i, j from all the involved quantities, given that we focus on a single mosaic.

As stated in the paper, we deal with counting rather than detection. Therefore, we do not know the exact nature of each inferred instance, *i.e.*, we cannot assign a correct/incorrect label to each different detected object. We can anyway directly estimate the total amount of true positives (TPs), false positives (FPs) and false negatives (FNs) by employing the counting model outputs. We perform the following assumption:

- For the positive image (the top one in the mosaic),

$$\text{TP}^{\text{pos}} = \begin{cases} c^{\text{pos}}, & \text{if } c^{\text{pos}} < \tilde{c} \\ \tilde{c}, & \text{otherwise} \end{cases}, \quad (7)$$

where \tilde{c} is the ground truth of the positive class. In fact, if the model predicts fewer objects than the ground truth, all the predicted objects are considered correct, and the remaining ones are FNs. Conversely, if the model predicts more objects than the ground truth, only \tilde{c} objects are correct, and the remaining contribute to the FPs. This situation for FNs and FPs can be directly derived from Eq. 7. Indeed, given that $c^{\text{pos}} = \text{FP}^{\text{pos}} + \text{TP}^{\text{pos}}$, it follows that

$$\text{FP}^{\text{pos}} = \begin{cases} 0, & \text{if } c^{\text{pos}} < \tilde{c} \\ c^{\text{pos}} - \tilde{c}, & \text{otherwise} \end{cases} \quad (8)$$

and provided that $\tilde{c} = \text{FN}^{\text{pos}} + \text{TP}^{\text{pos}}$, we also have

$$\text{FN}^{\text{pos}} = \begin{cases} \tilde{c} - c^{\text{pos}}, & \text{if } c^{\text{pos}} < \tilde{c} \\ 0, & \text{otherwise} \end{cases} \quad (9)$$

- For the negative image (the bottom one in the mosaic), the situation is simpler, given that all the contributions inferred by the model are FPs, as the TPs are identically zero, and thus also the FNs:

$$\text{TP}^{\text{neg}} = 0 \quad (10)$$

$$\text{FP}^{\text{neg}} = c^{\text{neg}} \quad (11)$$

$$\text{FN}^{\text{neg}} = 0 \quad (12)$$

With these quantities defined, we can introduce *counting precision* and *counting recall*, starting from their definitions in terms of TPs, FPs, and FNs.

A.1. Counting Precision

We start from the definition of precision, which is the following:

$$P = \frac{\text{TP}}{\text{TP} + \text{FP}} \quad (13)$$

Considering that the TPs and FPs are the sums of the respective contributions from the positive and negative parts of the mosaic – *i.e.* $\text{TP} = \text{TP}^{\text{pos}} + \text{TP}^{\text{neg}}$ and $\text{FP} = \text{FP}^{\text{pos}} + \text{FP}^{\text{neg}}$ – we obtain the precision expressed in terms of the quantities computed in Eqs. 7, 8, 10, and 11. Substituting and simplifying, we obtain

$$P = \begin{cases} \frac{c^{\text{pos}}}{c^{\text{pos}} + c^{\text{neg}}}, & \text{if } c^{\text{pos}} < \tilde{c} \\ \frac{\tilde{c}}{c^{\text{pos}} + c^{\text{neg}}}, & \text{otherwise} \end{cases} \quad (14)$$

which we can rewrite in simpler manner as

$$P = \frac{\min(c^{\text{pos}}, \tilde{c})}{c^{\text{pos}} + c^{\text{neg}}}. \quad (15)$$

This quantity is averaged among all the possible mosaics, which are $N(N - 1)$ (for each image, there are $N - 1$ possible mosaics), to obtain the final formula for the counting precision reported in the paper.

A.2. Counting Recall

The same idea used for deriving the counting precision can also be employed to compute the counting recall. The recall is defined as

$$R = \frac{TP}{TP + FN} \quad (16)$$

Even in this case, TPs and FNs are the sums of the respective contributions from the positive and negative parts of the mosaic – *i.e.* $TP = TP^{\text{pos}} + TP^{\text{neg}}$ and $FN = FN^{\text{pos}} + FN^{\text{neg}}$. We obtain the precision expressed in terms of quantities computed in Eqs. 7, 9, 10, and 12. Substituting and simplifying, we obtain

$$R = \begin{cases} \frac{c^{\text{pos}}}{\tilde{c}}, & \text{if } c^{\text{pos}} < \tilde{c} \\ 1, & \text{otherwise} \end{cases} \quad (17)$$

which we can rewrite as

$$R = \frac{\min(c^{\text{pos}}, \tilde{c})}{\tilde{c}}. \quad (18)$$

Again, this quantity is averaged in the same way as counting precision to obtain the final formula reported in the paper.

B. Derivation of Normalized Mean of Negative predictions (NMN)

NMN, as reported in the paper, is the absolute counting error computed by prompting the model with the negative classes normalized by the ground truth of the positive class. Formally, the main involved quantity computed for each image I_i prompted with the negative class P_j is given by

$$n_{ij} = \frac{|c_{ij} - \tilde{c}_{ij}^{\text{neg}}|}{\tilde{c}_i}, \quad i \neq j \quad (19)$$

where $\tilde{c}_{ij}^{\text{neg}}$ is the ground truth corresponding to the image prompted with the negative class, which is identically zero for $i \neq j$. Therefore, the numerator simplifies from $|c_{ij} - \tilde{c}_{ij}^{\text{neg}}|$ to c_{ij} (we assume the count predicted by the model is always positive). All the N_{ij} are then averaged over all the N images, each one prompted with all the possible $N - 1$ negative prompts:

$$\text{NMN} = \frac{1}{N} \sum_{i=1}^N \frac{1}{N-1} \sum_{\substack{j=1 \\ j \neq i}}^N n_{ij} \quad (20)$$

$$= \frac{1}{N} \sum_{i=1}^N \frac{1}{N-1} \sum_{\substack{j=1 \\ j \neq i}}^N \frac{c_{ij}}{\tilde{c}_i} \quad (21)$$

$$= \frac{1}{N(N-1)} \sum_{i=1}^N \frac{1}{\tilde{c}_i} \sum_{\substack{j=1 \\ j \neq i}}^N c_{ij} \quad (22)$$

which is the Eq. 2 reported in the paper.

C. DAVE Inference Details

We performed small changes to the inference code to prepare the DAVE model for our benchmark. This small update drastically improved DAVE on PrACo, unblocking its full potential.

Indeed, although DAVE has been designed to be resilient to images with multiple classes, the method assumes that it is prompted by one of the classes that are surely present in the image. In these cases, the model just considers the object class whose CLIP embedding is more similar to the provided prompt instead of allowing for zero matches based on a certain score threshold. If DAVE is prompted with a class not present in the one-class-only image, the original implementation ignores the CLIP-based proposal filtering. The outcome is catastrophic, especially for our *negative test*, as DAVE outputs the same count regardless of the input text prompt. For this reason, we modified DAVE to filter the proposals associated with the sole present cluster based on the input text. To compute the threshold to decide if the cluster proposals match the provided caption, we also fed the model with the positive class to have a CLIP upper-bound score as a reference. As in the original implementation, the proposals are kept if their CLIP score is higher than 85% of this reference CLIP score. Notice that this inference procedure would be difficult in real scenarios in which the positive class is not known a-priori. However, since the positive class can be obtained through image classification – and image classification is a well-established and solved problem in computer vision – we assume that, in real use-case scenarios, it is possible to derive a reliable positive class label using state-of-the-art image classifiers.

We also noticed that the outcome on our benchmark is very dependent on the clustering threshold τ used during the spectral clustering phase. Particularly, we observed that the original $\tau = 0.17$ was too high to correctly detect the two clusters corresponding to the two images in the mosaics. For this reason, in the main paper experiments, we set $\tau = 0.10$.

In Table 3, we report the model’s behavior with and without modification to the inference strategy and the original and changed τ parameter. As we can notice, the clustering threshold does not affect the negative test, where only one object cluster is always found. Our modification, which injects positive classes as a reference, originates a strong model from the negative test perspective, with an NMN of only 0.08. Concerning the mosaic model, the lowering of the *tau* threshold, together with the improved inference procedure, helps raise the counting precision and, in turn, the F1 by more than 12% with respect to the original implementation.

It is interesting to notice how these hyper-parameters

Table 3. We report the results for **DAVE** on the **test set** of FSC147, varying the clustering threshold τ (lowering it from the original 0.17 to 0.10, and modifying the inference procedure (*Mod. Inf.* column) obtained by feeding the model also with the reference positive class.

τ	Mod. Inf.	Negative Test		Mosaic Test			Classic	
		NMN ↓	PCCN ↑	CntP ↑	CntR ↑	CntF1 ↑	MAE ↓	RMSE ↓
0.17	✗	1.05	37.02	0.686	0.811	0.700	15.16	103.49
0.10	✗	1.05	37.02	0.743	0.805	0.732	15.16	103.49
0.17	✓	0.08	97.45	0.831	0.803	0.784	15.11	103.48
0.10	✓	0.08	97.62	0.843	0.799	0.790	15.23	103.53

have no effect on the class-specific classic counting metrics (MAE and RMSE), again proving the need for benchmarks like PrACo to effectively evaluate prompt-based counting models.

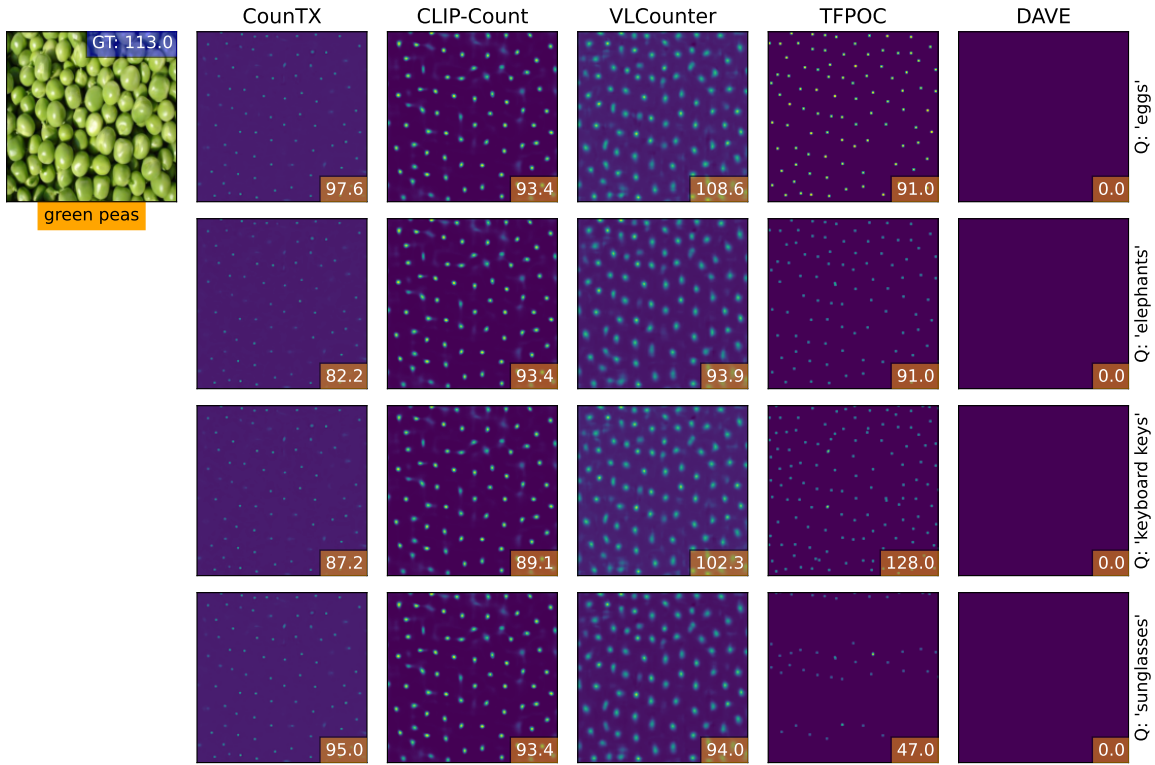
D. TFPOC Density Maps Creation

TFPOC is a training-free method that detects objects to count using the powerful SAM model [13]. Therefore, it is a detection-based model that counts the number of output detections. For this reason, it never really computes a density map, which is the main output interface used to prepare the predictions for the mosaic test and produce the qualitative visualization. To prepare the density maps, we simply plotted the region centers as small dots, each having an area of 1 (as is usually done for preparing ground truth density maps from dot annotations).

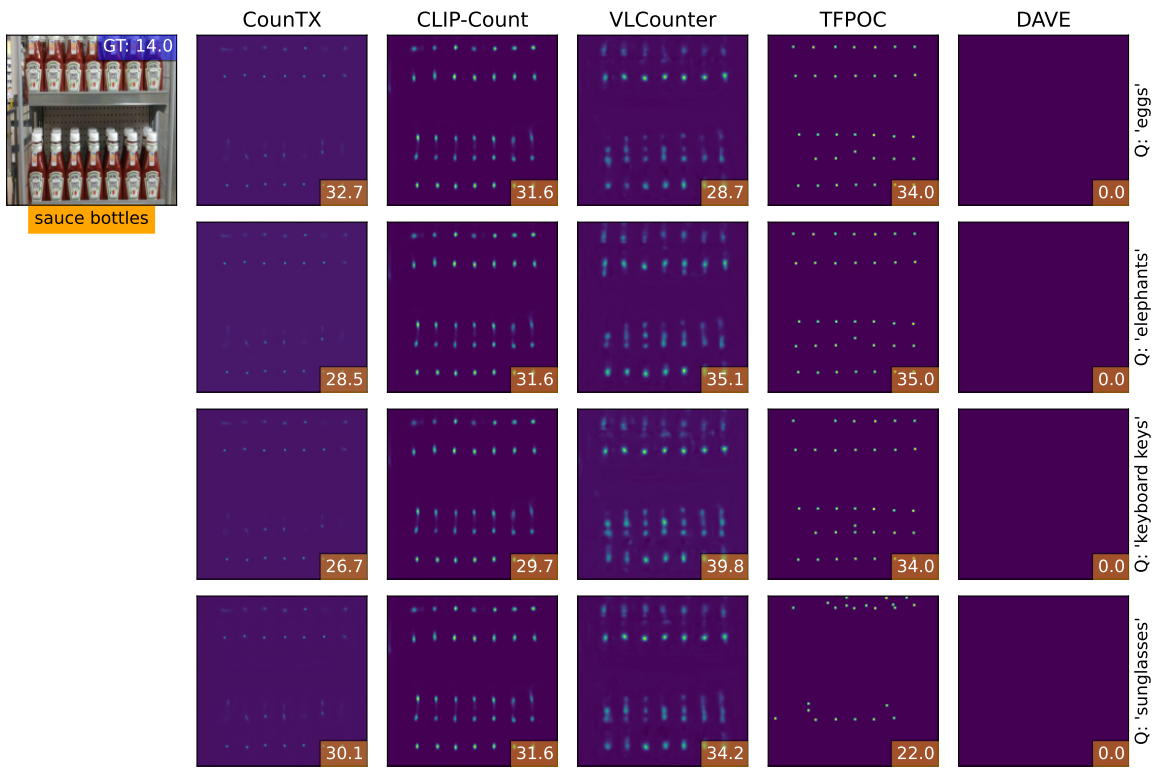
E. More Qualitative Results

In Figure 6, we report four images that we used to feed the model together with different negative classes. We can notice how all the methods except DAVE actually count the negative classes, predicting a number of instances comparable to – and in many cases even higher than – the ground truth of the positive class. Notice how DAVE identically predicts zero instances thanks to the proposed inference modification.

In Figure 7, we report more outcomes from the mosaic test. These further examples show how the models struggle to count only the correct class. Notably, despite DAVE being very good at distinguishing the only positive class from the negative test and achieving remarkable results on the PrACo metrics on the mosaic test, it still seems to sometimes catastrophically fail on the mosaic test, switching the correct class with the negative one.

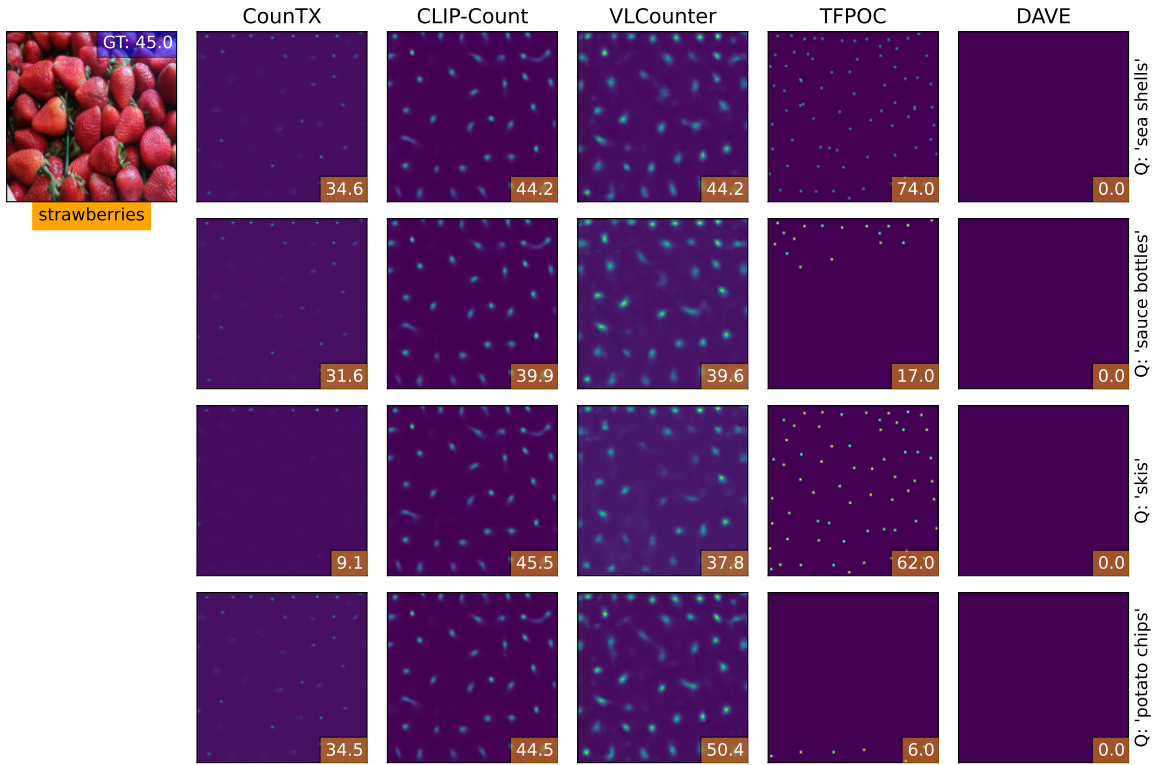


(a)

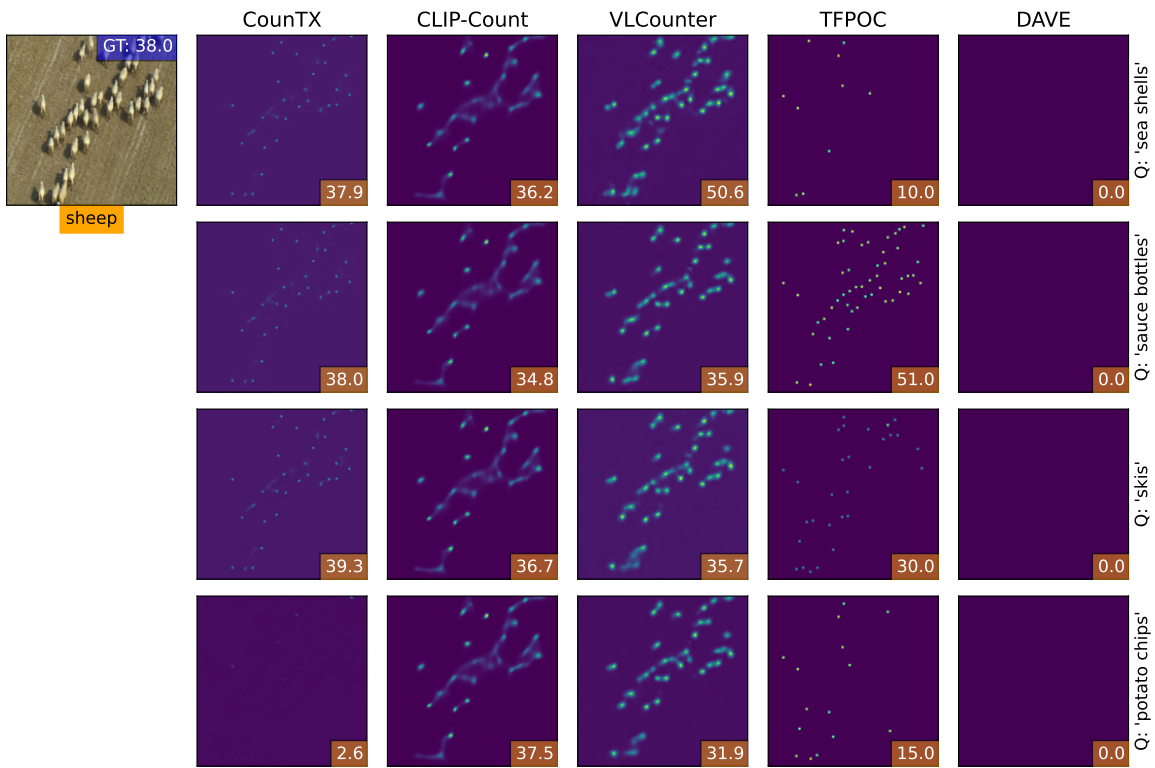


(b)

Figure 6. For each model, we report the density maps obtained when probing them with four different negative classes (*eggs*, *elephants*, *keyboard keys*, *sunglasses*) reported in the right-hand side of each row.



(c)



(d)

Figure 6. For each model, we report the density maps obtained when probing them with four different negative classes (*sea shells*, *sauce bottles*, *skis*, *potato chips*) reported in the right-hand side of each row (cont).

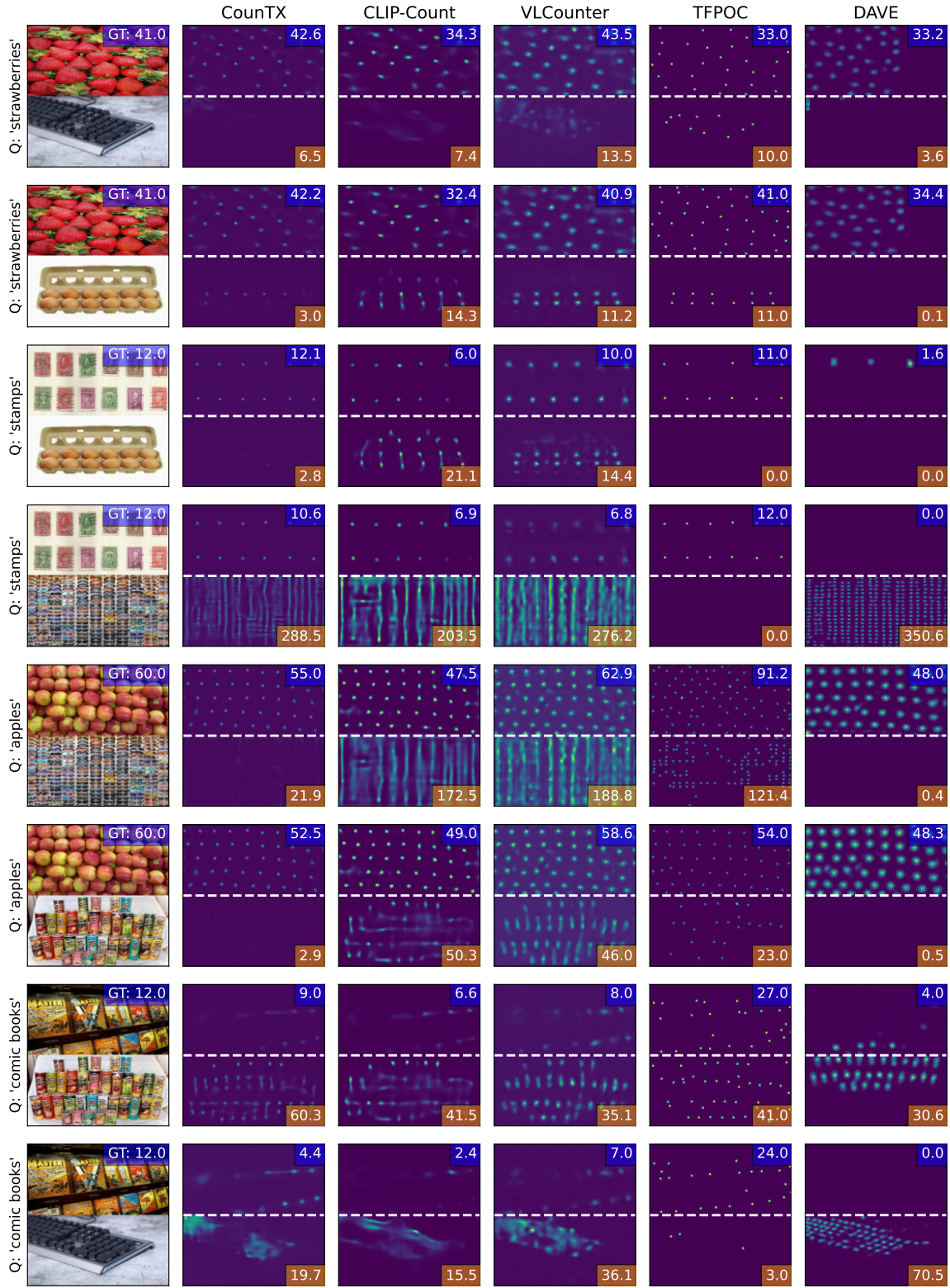


Figure 7. For each model, we report the output density maps for three different (*mosaic*, *input prompt*) pairs. In each figure, the count reported in the blue box is c_{ij}^{pos} , while the count reported in the red box corresponds to c_{ij}^{neg} .

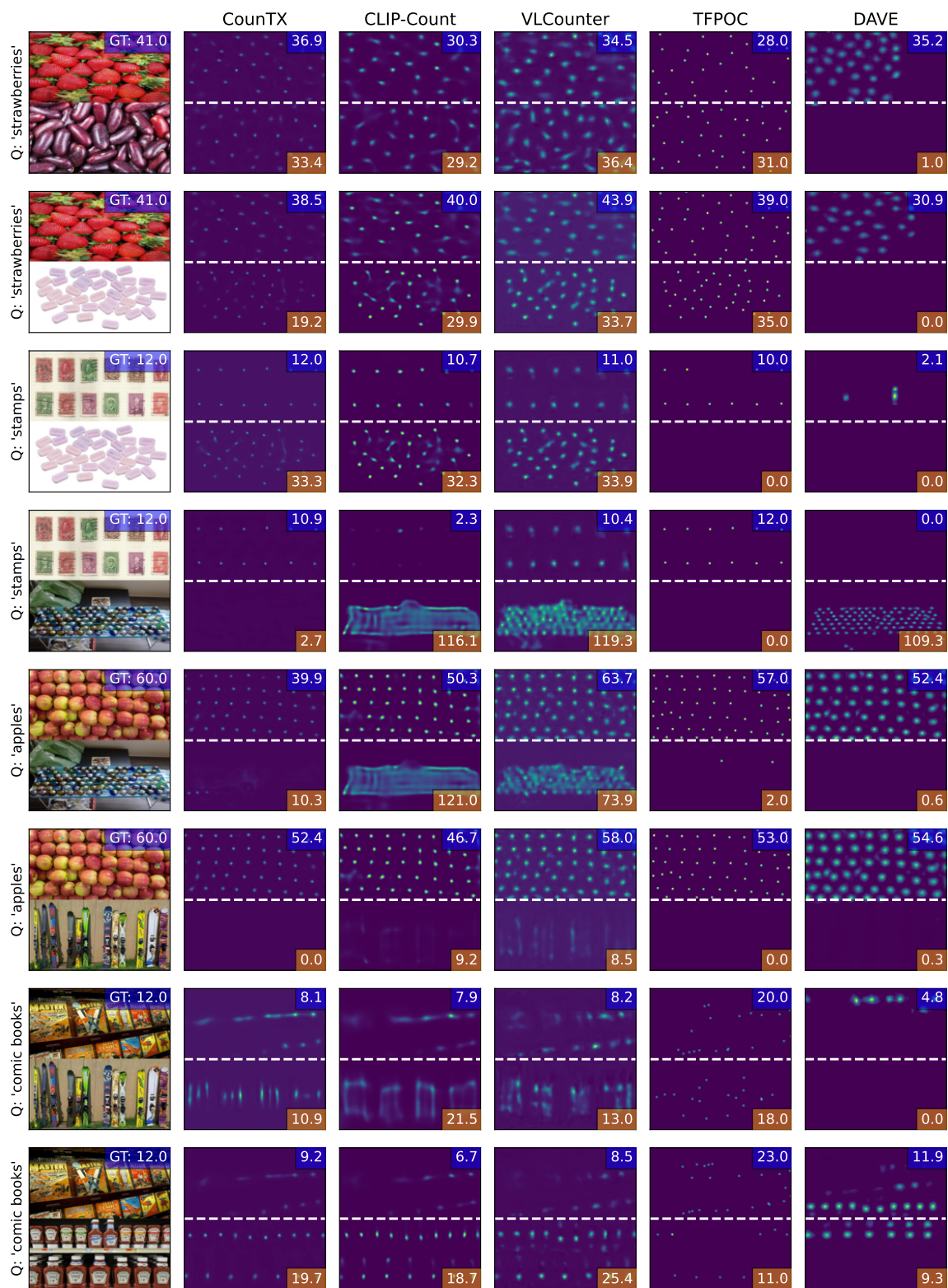


Figure 7. For each model, we report the output density maps for three different (*mosaic, input prompt*) pairs. In each figure, the count reported in the blue box is c_{ij}^{pos} , while the count reported in the red box corresponds to c_{ij}^{neg} (cont).